

The Transit Light Curve Project.

V. System Parameters and Stellar Rotation Period of HD 189733

Joshua N. Winn¹, Matthew J. Holman², Gregory W. Henry³, Anna Roussanova¹,
Keigo Enya⁴, Yuzuru Yoshii^{5,6}, Avi Shporer⁷, Tsevi Mazeh⁷,
John Asher Johnson⁸, Norio Narita⁹, Yasushi Suto⁹

ABSTRACT

We present photometry of HD 189733 during eight transits of its close-in giant planet, and out-of-transit photometry spanning two years. Using the transit photometry, we determine the stellar and planetary radii and the photometric ephemeris. Outside of transits, there are quasiperiodic flux variations with a 13.4 day period that we attribute to stellar rotation. In combination with previous results, we derive upper limits on the orbital eccentricity, and on the true angle between the stellar rotation axis and planetary orbit (as opposed to the angle between the projections of those axes on the sky).

Subject headings: planetary systems — planetary systems: formation — stars: individual (HD 189733) — stars: rotation

1. Introduction

For the same reason that eclipsing binary stars are important in stellar astrophysics, transiting planets play an outsized role in exoplanetary science. This can be appreciated by comparing the

¹Department of Physics, and Kavli Institute for Astrophysics and Space Research, Massachusetts Institute of Technology, Cambridge, MA 02139, USA

²Harvard-Smithsonian Center for Astrophysics, 60 Garden Street, Cambridge, MA 02138, USA

³Center of Excellence in Information Systems, Tennessee State University, 3500 John A. Merritt Blvd., Box 9501, Nashville, TN 37209, USA

⁴Institute of Space and Astronautical Science, Japan Aerospace Exploration Agency, 3-1-1, Yoshinodai, Sagami-hara, Kanagawa, 229-8510, Japan

⁵Institute of Astronomy, School of Science, University of Tokyo, 2-21-1 Osawa, Mitaka, Tokyo 181-0015, Japan

⁶Research Center for the Early Universe, School of Science, University of Tokyo, 7-3-1 Hongo, Bunkyo-ku, Tokyo 113-0033, Japan

⁷Wise Observatory, Raymond and Beverly Sackler Faculty of Exact Sciences, Tel Aviv University, Tel Aviv 69978, Israel

⁸Department of Astronomy, University of California, Mail Code 3411, Berkeley, CA 94720, USA

⁹Department of Physics, The University of Tokyo, Tokyo 113-0033, Japan

transiting exoplanet HD 189733b (Bouchy et al. 2005), the subject of this paper, to the arbitrarily chosen non-transiting planet HD 187123b (Butler et al. 1998). Both planets are “hot Jupiters” detected by the Doppler method. All that is known about HD 187123b is its orbital period ($P = 3.097$ days) and minimum mass ($M_p \sin i = 0.52 M_{\text{Jup}}$), despite 6 years having elapsed since its discovery. In contrast, for HD 189733b, discovered only 1.5 yr ago, transit photometry has revealed the planet’s radius ($1.15 R_{\text{Jup}}$; Bouchy et al. 2005, Bakos et al. 2006a) and removed the $\sin i$ ambiguity in the planet’s mass ($M_p = 1.13 M_{\text{Jup}}$). Infrared photometry during a secondary eclipse has led to a determination of the planet’s $16 \mu\text{m}$ brightness temperature ($T_p = 1300 \text{ K}$; Deming et al. 2006). Most recently, spectroscopic observations during a transit have shown that the angle on the sky between the orbit normal and the stellar rotation axis is within a few degrees of zero (Winn et al. 2006).

These measurements are essential for a complete understanding of the atmospheres and interiors of hot Jupiters, as well as their formation and migration mechanisms. An even richer set of measurements can be expected in the future, from investigators pursuing transmission spectroscopy, reflected-light observations, and other transit-related investigations (as reviewed recently by Charbonneau et al. 2006a). One goal of the Transit Light Curve (TLC) Project is to support these efforts by refining the estimates of the planetary, stellar, and orbital parameters, through high-accuracy, high-cadence photometry of exoplanetary transits. We also seek to measure or bound any variations in the transit times and light-curve shapes that would be caused by the influence of additional bodies in the system (Miralda-Escudé 2002; Agol et al. 2005; Holman & Murray 2005). Along the way, we are exploring different techniques for photometry and parameter determination. Previous papers in this series have reported results for the exoplanets XO-1b (Holman et al. 2006a), OGLE-TR-111b (Winn et al. 2007), TrES-1 (Winn, Holman, & Roussanova 2006), and OGLE-TR-10b (Holman et al. 2006b).

This paper presents our results for HD 189733b, along with out-of-transit photometry spanning two years. The reason for gathering out-of-transit photometry was to attempt to measure the stellar rotation period. The parent star is relatively active, with a chromospheric activity index $S = 0.525$ (Wright et al. 2004) and $\log R'_{HK} = -4.4$, raising the possibility of measuring the rotation period through starspot-induced quasiperiodic flux variations. As we will explain, the measurements of both the rotation period and the Rossiter-McLaughlin effect permit the determination of the true angle between the orbit normal and stellar rotation axis (as opposed to the angle between the projections of those vectors on the sky, which was measured by Winn et al. 2006).

This paper is organized as follows. In § 2, we present photometry of 8 different transits, along with nightly photometry over two consecutive observing seasons. In particular, § 2.2 presents the out-of-transit photometry and the estimation of the stellar rotation period. In § 3, we describe the parametric model that was fitted to the data, and in § 4 we present the results for the planetary, stellar, and orbital parameters, as well as the new transit ephemerides, a limit on the orbital eccentricity, and the three-dimensional spin-orbit alignment. The last section is a summary.

2. Observations and Data Reduction

Our observations took place in 2005 and 2006 using telescopes at 4 different observatories. Each of the sections below presents the photometry from a given observatory. All together, we observed 8 different transits. Table 1 gives a summary of the characteristics of the data from each transit, and Table 2 gives the final photometry. A telescope at Fairborn Observatory (§ 2.2) was also used to monitor the out-of-transit flux of HD 189733 over the two observing seasons.

2.1. Fred Lawrence Whipple Observatory

We observed the transits of UT 2006 Jul 21 and Sep 10 with the 1.2m telescope at the Fred L. Whipple Observatory on Mt. Hopkins, Arizona.¹ We used KeplerCam, which has one 4096² Fairchild 486 back-illuminated CCD, with a 23'.1 × 23'.1 field of view. For our observations we used 2 × 2 binning, which gives a scale of 0''.68 per binned pixel, a readout and setup time of 11 s, and a typical readout noise of 7 e⁻ per binned pixel. We observed both transits through the SDSS *z* band filter, in order to minimize the effect of color-dependent atmospheric extinction on the relative photometry and to minimize the effect of limb-darkening on the transit light curve. We deliberately defocused the telescope such that the full-width at half-maximum (FWHM) of stellar images was about 7 binned pixels (4''.8) in order to permit a consistent exposure time of 5 s. We used automatic guiding to keep the image registration as constant as possible. We also obtained dome flat exposures and zero-second (bias) exposures at the beginning and the end of each night.

On UT 2006 Jul 21, the sky conditions began partly cloudy but gradually improved as the night went on. We observed the target star as it rose from an airmass of 1.19 to 1.01 and then descended to an airmass of 1.23. There was a 15-minute interruption after second contact, due to clouds. On UT 2006 Sep 10, the sky conditions were mainly clear (but not all-sky photometric). We followed the target star from an airmass of 1.02 to 2.5, although we discarded the data taken at airmass > 1.9 because of their much poorer quality. There was a 15-minute interruption prior to third contact, due to a computer crash, which also caused a change in image registration and focus.

We used standard IRAF² procedures for the overscan correction, trimming, bias subtraction, and flat-field division. We performed aperture photometry of HD 189733 and 14 nearby and necessarily fainter stars. The light curve of each comparison star was normalized to have unit median, and the mean of these normalized light curves was taken to be the comparison signal. The light curve of HD 189733 was divided by the comparison signal, and corrected for residual

¹The data from the first of these two transits have already been presented by Winn et al. (2006).

² The Image Reduction and Analysis Facility (IRAF) is distributed by the National Optical Astronomy Observatories, which are operated by the Association of Universities for Research in Astronomy, Inc., under cooperative agreement with the National Science Foundation.

systematic effects by dividing out a linear function of time. The zero point and slope of the linear function were determined as part of the model-fitting procedure, as explained in § 4. Figure 1 shows the final light curves, along with a time-averaged composite light curve created from the two data sets.

2.2. Fairborn Observatory

We used the T10 0.8m automated photometric telescope (APT) at Fairborn Observatory, in Arizona, to observe four complete transits of HD 189733b and to monitor the out-of-transit stellar flux. The T10 APT is equipped with a two-channel precision photometer employing two EMI 9124QB bi-alkali photomultiplier tubes to make simultaneous measurements in the Strömgren b and y passbands. The APT measures the difference in brightness between a program star and a nearby constant comparison star (or stars) with a typical precision of 0.0015 mag for bright stars ($V < 8.0$). For the HD 189733 transits, we used the comparison star HD 189410 ($V = 5.68$, $B - V = 0.34$, F0). The differential magnitudes were reduced with nightly extinction coefficients and transformed to the Strömgren system with yearly mean transformation coefficients. To improve our photometric precision, we combined the separate b and y differential magnitudes into a single $(b + y)/2$ passband. For additional information on the telescopes, photometers, observing procedures, and data reduction techniques, see Henry (1999) and Eaton, Henry, & Fekel (2003).

We observed the transits of UT 2005 Nov 28, 2006 May 2, 2006 May 22, and 2006 Jun 11. On each of those nights, the differential magnitude of HD 189733 was recorded for 3-5 hours bracketing the expected time of mid-transit. The transit light curves are shown in the top 4 panels of Fig. 2. Like the FLWO data, these data have been corrected by a linear function of time that was determined as part of the fitting procedure (see § 4).

In addition, we also measured the out-of-transit flux with the APT on 93 different nights spanning two observing seasons between 2005 October and 2006 July. Three comparison stars were observed on each night. The out-of-transit flux measurements are shown in the top two panels of Fig. 3. The flux varied erratically during the 2005 observing season and at the beginning of the 2006 season. However, a quasiperiodic signal became evident near the end of our 2006 season observations with a peak-to-peak amplitude of 1.3% and a period of about 13 days, although only 2.5 cycles were observed.

This type of photometric behavior—erratic and occasionally quasiperiodic variation—is common among chromospherically active stars, especially stars with low or intermediate levels of activity (see, e.g., Henry, Fekel, & Hall 1995). The photometric variability in these stars arises from photospheric starspots and plages that are carried into and out of view by the stellar rotation. In the case of HD 189733, the spots cover only $\sim 1\%$ of the stellar surface at any moment, and their distribution on the star changes significantly on the rotational timescale. A periodogram of the quasiperiodic portion of the light curve (indicated by the solid dots in the middle panel of Fig. 3)

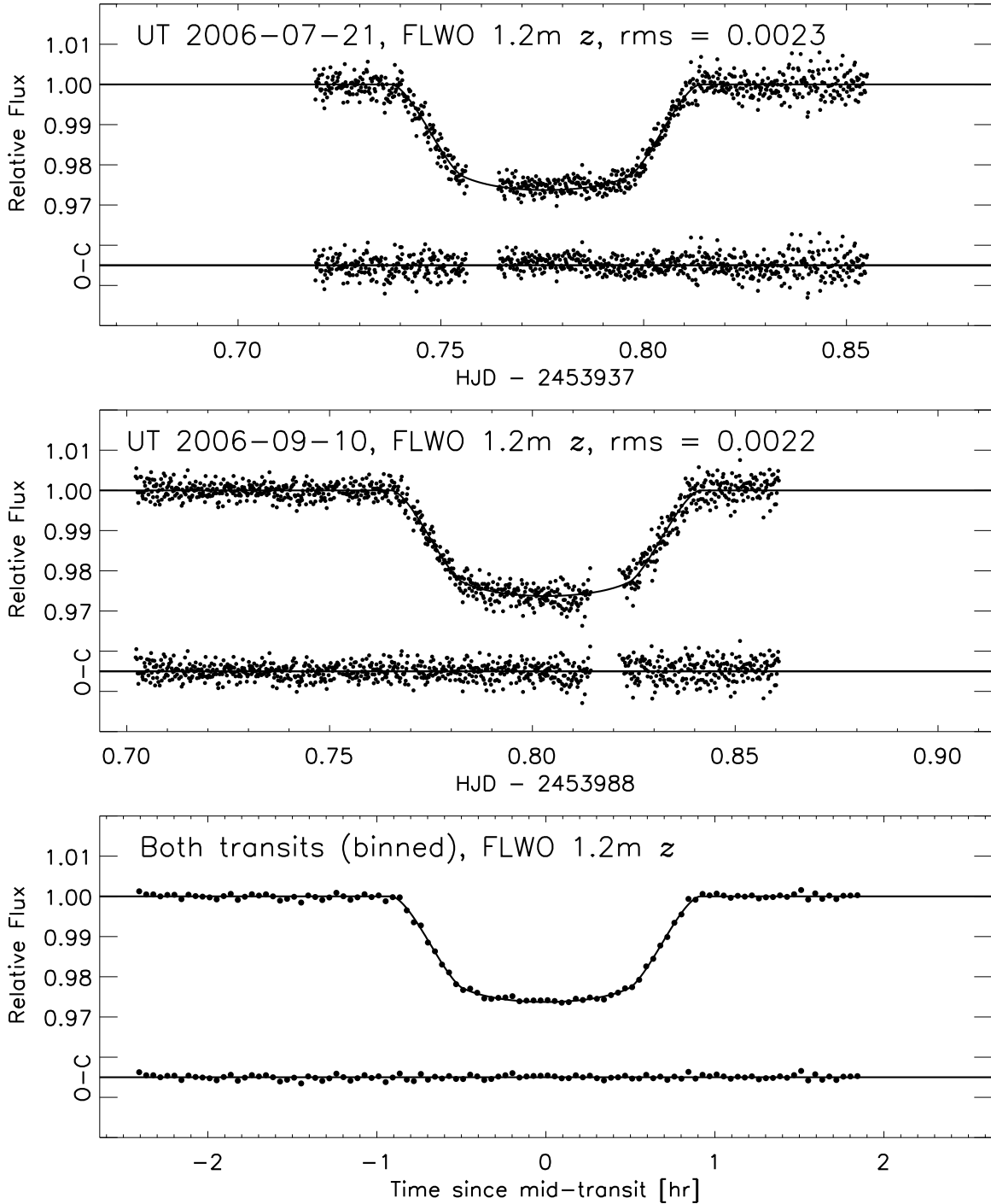


Fig. 1.— Photometry of HD 189733 in the z band, using the FLWO 1.2m telescope and Keplercam. These data were used to estimate the planetary, stellar, and orbital parameters (see § 3). The bottom panel is a composite light curve created from both data sets, after time-shifting the earlier transit and averaging into 1 minute bins. The residuals (observed–calculated) are plotted beneath the data.

shows a strong peak at 13.4 days, which we take to be the stellar rotation period. We estimated the uncertainty by recalculating the light curve using each of the three different comparison stars; the standard deviation of the results was 0.4 days. Thus, in what follows, we adopt the value $P_{\text{rot}} = 13.4 \pm 0.4$ days. Since this result is only based on 2.5 cycles, continued observations are warranted to check our estimate. There may be additional errors because of differential rotation and the variations in spot positions and intensities on the rotational timescale. The bottom panel of Fig. 3 shows the flux as a function of rotational phase during the epoch of quasiperiodic variation. A periodogram of the entire data set also shows a peak at 13.4 days, along with a peak at 6.7 days, presumably from a time period when star spots occurred on both sides of the star.

2.3. MAGNUM Observatory

We observed the transit of UT 2006 Aug 21 with the 2m telescope at the Multi-color Active Galactic Nuclei Monitoring (MAGNUM) observatory on Haleakala, Hawaii (Kobayashi et al. 1998; Yoshii 2002; Yoshii, Kobayashi, & Minezaki 2003). This is the same transit that was observed spectroscopically by Winn et al. (2006). We used the multi-color imaging photometer (MIP), which allows for simultaneous observation with an optical 1024² SITE CCD and an infrared SBRC InSb 256² detector. In this case, we used only the optical detector, because the infrared detector was saturated even in very short exposures. We observed in the *V* band. Because the MIP field of view is only $1'.5 \times 1'.5$, and there are no good comparison stars within this small field, we nodded repeatedly between the target star and a calibration star, with 1 s exposures. The calibration star was HD 190449 ($V = 8.12$, $B - V = 0.79$, K0). The average interval between exposures of HD 189733 was 46 s. The median FWHM of stellar images was $1''.2$.

We reduced the images with the standard MIP pipeline described by Minezaki et al. (2004). We then performed aperture photometry on HD 189733 and HD 190449, using an aperture radius of $6''.65$ and a sky annulus ranging in radius from $6''.65$ to $9''.42$. To produce a comparison signal, the time series for HD 190449 was boxcar-smoothed (with a width of 4 points, or 3 minutes) and then linearly interpolated onto the time stamps of the HD 189733 data. Then the HD 189733 time series was divided by this comparison signal. A few extreme outlying points were rejected. To remove residual systematic errors in the out-of-transit flux determination, we divided by a linear function of time that was determined as part of the fitting procedure (see § 4). The final light curve is shown in the fifth panel of Fig. 2.

2.4. Wise Observatory

We observed the transit of 2006 Sep 5 with the 1m telescope at Wise Observatory, in Israel. We used a Tektronix 1024² back-illuminated CCD detector, giving a pixel scale of $0''.7$ and a field of view of $11'.9 \times 11'.9$. We observed through a Johnson *I* filter, the reddest optical band available

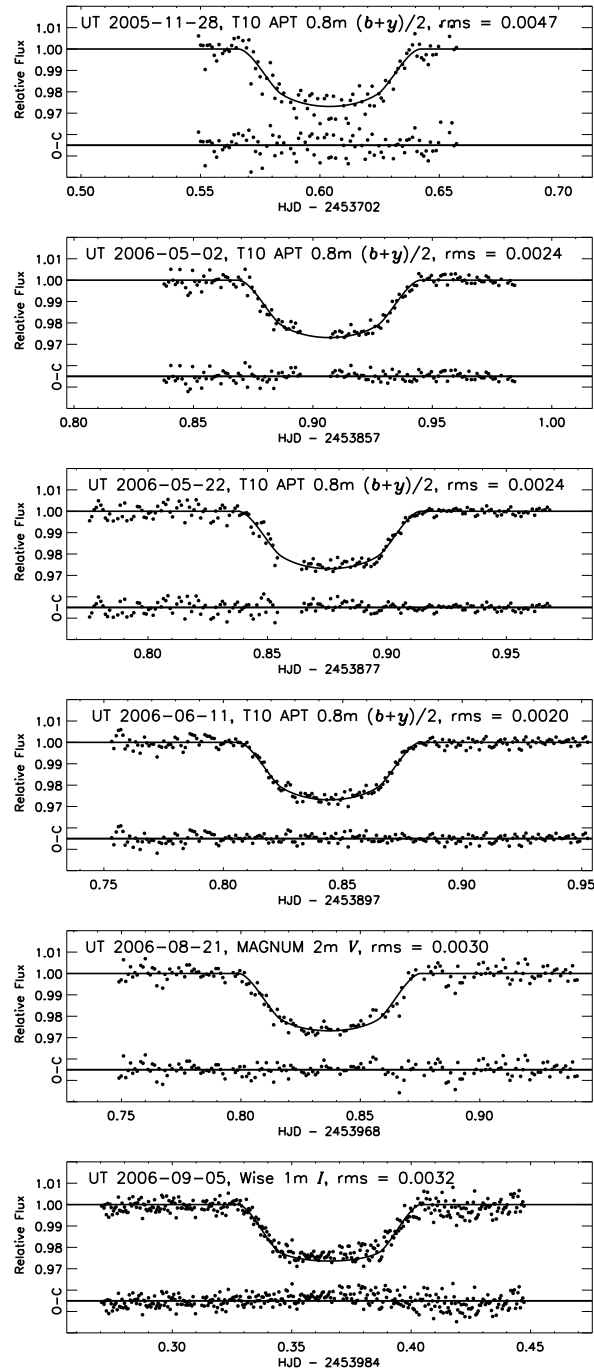


Fig. 2.— Relative photometry of HD 189733 during 6 different transits. The date, telescope, and filter are identified on each panel. These data were used only for measurements of the times of transit (see § 3). The model, shown as the solid line, is based on the model derived from the FLWO z -band data after changing the limb-darkening parameters appropriately. In all cases, the residuals (observed–calculated) are plotted beneath the data.

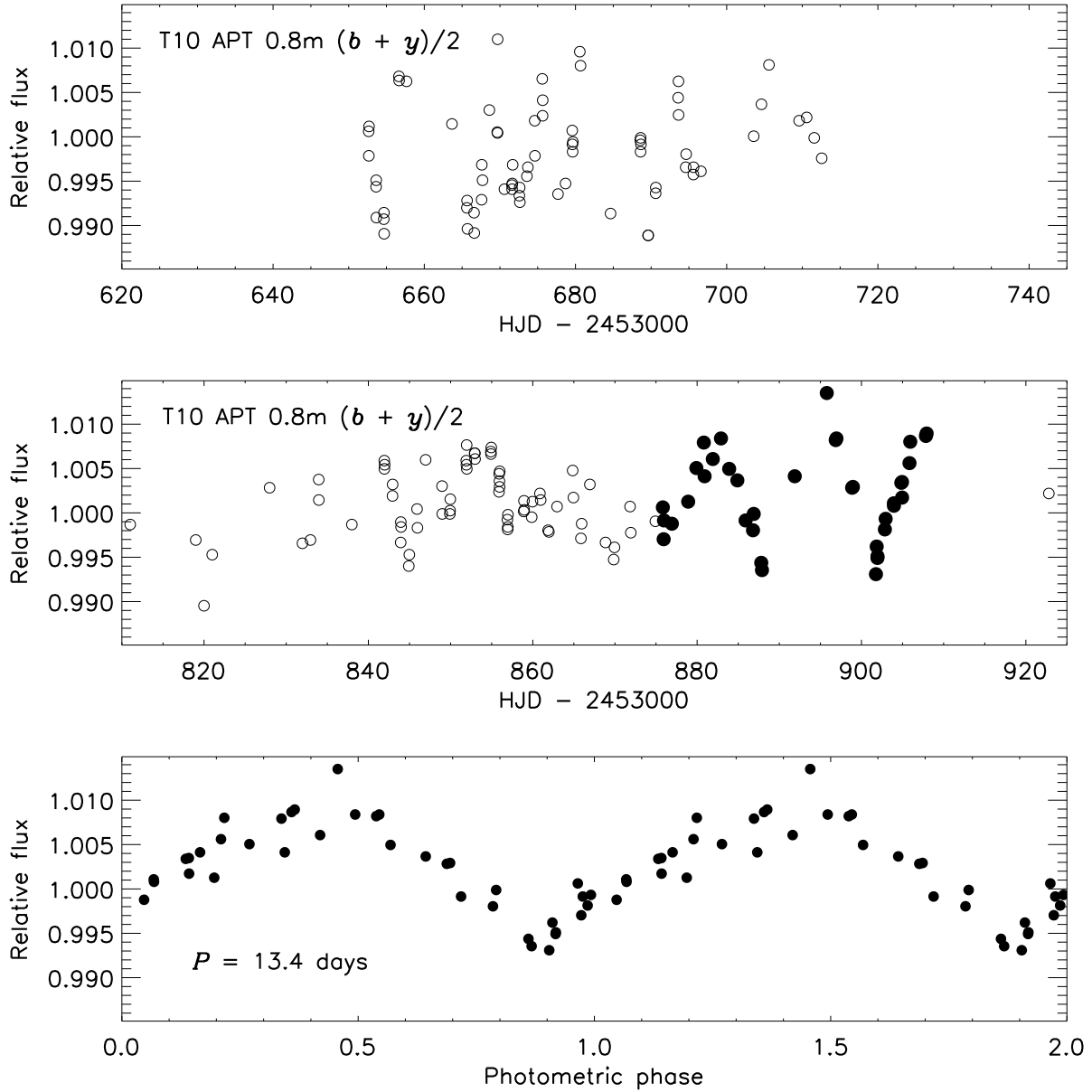


Fig. 3.— Relative photometry of HD 189733, from the T10 0.8m APT at Fairborn Observatory. The top two panels show data from the 2005 and 2006 observing seasons, respectively. The solid symbols show the portion of data that was used in the periodogram analysis. This subset of the data is plotted in the bottom panel as a function of the photometric phase.

on this camera. The exposure time was 10 s and the telescope was defocused in order to avoid saturation. Autoguiding was used to keep the image registration constant throughout the night. We also obtained sky flat exposures at sunset and zero-second (bias) exposures at the beginning and during the night. We performed the data reduction and photometry using very similar procedures to those that were used on the FLWO data (§ 2.1). The bottom panel of Fig. 2 shows the final light curve.

3. Determination of System Parameters

To estimate the planetary, stellar, and orbital parameters, and the times of transit, we fitted a parameterized model to the transit photometry. The model and the fitting method were similar to those described in previous TLC papers (see, e.g., Winn et al. 2007), except that in this case we accounted for correlated noise, as described below. The model is based on a Keplerian orbit of a star (with mass M_\star and radius R_\star) and a single planet (M_p , R_p) about their center of mass. For most of the analysis we assumed that the orbital eccentricity e is zero, because the expected timescale of tidal circularization is short in the absence of excitations from other planets (see, e.g., Rasio et al. 1996, Trilling et al. 2000, Dobbs-Dixon et al. 2004, Adams & Laughlin 2006). However, in § 4.3, we discuss the empirical upper limits on the orbital eccentricity. The orbit has a period P and an inclination i relative to the sky plane. We define the coordinate system such that $0^\circ \leq i \leq 90^\circ$. It is often useful to refer to the impact parameter $b \equiv a \cos i / R_\star$ (where a is the semimajor axis) rather than the inclination.

Because one of our goals was to measure the individual transit times, we allowed each transit to have an independent value of T_c , the transit midpoint, rather than forcing them to be separated by exact multiples of the orbital period. Thus, the only effect of P on the model is to determine the semimajor axis a for a given value of the total mass. We fixed $P = 2.218575$ days, the value determined by Bouchy et al. (2005) and Hébrard & Lecavelier Des Etangs (2006) from the detection of transits in the *Hipparcos* database. The uncertainty of 0.000003 days was negligible for our purposes, although we were able to use the resulting values of T_c to produce an independent estimate of the period, as described in § 5.

Neither M_\star nor M_p can be determined from photometry alone. As we have done in previous TLC analyses, we fixed M_\star at a value that is based on an analysis of the stellar spectrum and other observable properties. We then used the scaling relations $R_p \propto M_\star^{1/3}$ and $R_\star \propto M_\star^{1/3}$ to estimate the systematic error associated with the uncertainty in M_\star . In this case we adopted the value $M_\star = 0.82 \pm 0.03 M_\odot$ (Bouchy et al. 2005). The planetary mass M_p hardly affects the photometric model at all, but for completeness we used the value $M_p = 1.13 M_{\text{Jup}}$ (Winn et al. 2006).

To calculate the relative flux as a function of the projected separation of the planet and the star, we employed the analytic formulas of Mandel & Agol (2002) to compute the integral of the intensity over the unobscured portion of the stellar disk. We assumed the limb darkening law to

be quadratic,

$$\frac{I\mu}{I_1} = 1 - u_1(1 - \mu) - u_2(1 - \mu)^2, \quad (1)$$

where I is the intensity, and μ is the cosine of the angle between the line of sight and the normal to the stellar surface. We fixed the limb-darkening coefficients at the values calculated by Claret (2000, 2004) for observations of a star with the observed spectral properties.³ We also investigated the effect of fitting for the limb darkening parameters, as discussed below. In addition, the light curves exhibited gradients in the out-of-transit data, probably due to differential extinction between the target star and the comparison stars, or some other systematic error. For this reason, each of the 8 data sets was modeled with two extra parameters: the out-of-transit flux f_{oot} and a time gradient α .

The fitting statistic was

$$\chi^2 = \sum_{j=1}^{N_f} \left[\frac{f_j(\text{obs}) - f_j(\text{calc})}{\sigma_j} \right]^2, \quad (2)$$

where $f_j(\text{obs})$ is the flux observed at time j , σ_j controls the relative weights of the data points, and $f_j(\text{calc})$ is the calculated value. In order to derive realistic uncertainties on the parameters, it is important for σ_j to include not only measurement errors but also any unmodeled systematic effects. Of particular importance is the timescale of the systematic effects. Correlated noise effectively reduces the number of independent data points and correspondingly increases the uncertainties in the model parameters, an issue that Pont et al. (2006) and Gillon et al. (2006) have recently brought to attention in the context of transit photometry.

Our approach to this problem was as follows. First, for each of the 8 transits, we rescaled the instrumental uncertainties such that $\chi^2/N_{\text{dof}} = 1$ for the best-fitting model. The resulting uncertainties are those that are given in Table 2. Second, we followed the procedure of Gillon et al. (2006) to decompose the observed noise into “white noise” (that which averages down as $1/\sqrt{N}$, where N is the number of data points) and “red noise” (that which does not average down over some specified time interval). Specifically, we calculated the standard deviation of the residuals (σ) and the standard deviation of the time-averaged residuals (σ_N). The averaging time was 1 hr (a timescale comparable to the transit event), corresponding to a number N of data points that depended upon the cadence of observations. Then we solved for the white noise σ_w and red noise σ_r from the system of equations

$$\sigma_1^2 = \sigma_w^2 + \sigma_r^2, \quad (3)$$

$$\sigma_N^2 = \frac{\sigma_w^2}{N} + \sigma_r^2. \quad (4)$$

Finally, to account approximately for the effective reduction in the number of independent data points, we rescaled the σ_j in Eq. (2) by the factor $\sigma_r/(\sigma_w/\sqrt{N})$.

³Specifically, we used the tabulated values for an ATLAS model with $T_{\text{eff}} = 5000$ K, $\log g = 4.5$ (cgs), $\log [M/H] = 0.0$ and $v_t = 2.0$ km s⁻¹. For the z band, $u_1 = 0.32$ and $u_2 = 0.27$.

The results for σ_w , σ_r , and the rescaling factor for each data set are given in Table 1. These results are not very sensitive to the choice of averaging time. Any choice between 15 min and a few hours gave similar results. Among the data sets are wide disparities in the degree of red noise, ranging over a factor of 10. By far the best data, in the sense of the smallest noise correlations, are from the FLWO 1.2m telescope and Keplercam (§ 2.1). For this reason, we decided to estimate the system parameters using *only* the FLWO data, and use the other data sets only to determine transit times and as a consistency check on the FLWO results. (Had we included the other data sets, their statistical weight would anyways have been much smaller.)

In short, we used the FLWO data to solve for the two bodies’ radii (R_\star and R_p); the orbital inclination (i); and the mid-transit time (T_c), the out-of-transit flux (f_{out}), and a time gradient (α) for each of the 2 transits. We then fixed R_\star , R_p , and i at the best-fitting values, and fitted each of the remaining 6 data sets to find T_c , f_{out} , and α .

To solve for the model parameters and their uncertainties, we used a Markov Chain Monte Carlo algorithm (see, e.g., Tegmark 2004). Our jump function was the addition of a Gaussian random number to each parameter value. We set the perturbation sizes such that $\sim 20\%$ of jumps are executed. We created 10 independent chains, each with 500,000 points, starting from random initial positions, and discarded the first 20% of the points in each chain. The Gelman & Rubin (1992) R statistic was within 0.2% of unity for each parameter, a sign of good mixing and convergence. We merged the chains and took the median value of each parameter to be our best estimate, and the standard deviation as the 1σ uncertainty.

4. Results

The results are given in Table 3. Along with the results for the model parameters, we have provided results for some useful derived quantities such as the impact parameter b , the radius ratio (R_p/R_\star), and the fraction $(R_p/a)^2$ (which gives the fraction of starlight reflected by the planet, for an albedo of unity). We also report the calculated values of the full transit duration (the time between first and fourth contact, $t_{\text{IV}} - t_{\text{I}}$), and the partial transit duration (the time between first and second contact, or between third and fourth contact).⁴

4.1. Stellar and Planetary Radii

The result for the stellar radius is $R_\star = 0.753 \pm 0.025 R_\odot$. The uncertainty is dominated by the statistical error of $0.023 R_\odot$ (3.1%). The covariance with the uncertainty in the stellar mass produces an additional error of $0.009 R_\odot$ (1.2%), which we have added in quadrature to the

⁴Although the partial transit duration is listed as $t_{\text{II}} - t_{\text{I}}$ in Table 3, all of the results in Table 1 are based on the entire light curves, including both ingress and egress data. Our model assumes $t_{\text{II}} - t_{\text{I}} = t_{\text{IV}} - t_{\text{III}}$.

statistical error to arrive at the net uncertainty of $0.025 R_{\odot}$. We find the planetary radius to be $R_p = 1.156 \pm 0.046 R_{\text{Jup}}$, where the uncertainty is again dominated by the statistical error of $0.044 R_{\text{Jup}}$.

To test the robustness of these results, we performed some additional fits. We gauged the importance of the choice of limb-darkening law by re-fitting the data under different assumptions. When we allowed the limb-darkening coefficients u_1 and u_2 to be free parameters rather than holding them fixed, we found $R_{\star} = 0.755 R_{\odot}$ and $R_p = 1.163 R_{\text{Jup}}$, well within the 1σ error of our original analysis. (The optimized limb-darkening coefficients for the z band were $u_1 = 0.35$ and $u_2 = 0.22$, as compared to the theoretical values of $u_1 = 0.32$ and $u_2 = 0.27$.) Likewise, the results changed by only 0.25σ when we used a linear limb-darkening law ($u_2 = 0$), regardless of whether the linear limb-darkening coefficient was fixed or taken to be a free parameter. As another check, we fitted each of the 8 transit data sets separately, solving for the parameters $\{R_{\star}, R_p, i, T_c, \alpha, f_{\text{out}}\}$ in each case. Although the statistical power of the FLWO photometry was the greatest, as noted previously, all 8 sets of results agreed within their calculated error bars. In particular, the unweighted “ensemble averages” of the results from the 6 non-FLWO data sets were $R_{\star} = 0.760 R_{\odot}$ and $R_p = 1.148 R_{\text{Jup}}$, again in agreement with our original analysis.

How do these results compare to the previous analyses of HD 189733 by Bouchy et al. (2005) and Bakos et al. (2006a)? An important difference is that those authors decided not to determine R_{\star} from the transit photometry.⁵ Rather, those authors used estimates of R_{\star} based on an analysis of other observable properties of the star. Bouchy et al. (2005) used measurements of the star’s parallax, effective temperature, surface gravity, and metallicity, in comparison with the outputs of stellar evolution models, and concluded $R_{\star} = 0.76 \pm 0.01 R_{\odot}$. Likewise, Bakos et al. (2006a) investigated four different ways of determining the stellar radius, based on broad band colors, spectral properties, and model isochrones, and found a stellar radius in the range $0.74\text{--}0.79 R_{\odot}$. Ultimately, Bakos et al. (2006a) adopted the value $0.758 \pm 0.016 R_{\odot}$ based on a calibration of 2MASS photometry by Masana et al. (2006). Our determination of R_{\star} based on the transit light curve is in agreement with those independent determinations; the mutual agreement constitutes an important consistency check on the data and our analysis.

Our value for the planetary radius agrees with the value $R_p = 1.154 \pm 0.033 R_{\text{Jup}}$ found by Bakos et al. (2006a). While the Bakos et al. (2006a) result would appear to be more precise, the comparison is somewhat misleading because Bakos et al. (2006a) were not simultaneously fitting for R_{\star} , as noted above. If we follow their procedure of fixing $R_{\star} = 0.758 \pm 0.016 R_{\odot}$, then our result for the planetary radius becomes more precise: $R_p = 1.164 \pm 0.028 R_{\text{Jup}}$. Both our result and that of Bakos et al. (2006a) disagree with that of Bouchy et al. (2005), who found $1.26 \pm 0.03 R_{\text{Jup}}$ based on a B -band light curve from the 1.2m telescope at the Observatoire de Haute-Provence (OHP).

⁵While Bakos et al. (2006a) did fit for the stellar radius, finding $R_{\star} = 0.68 \pm 0.02 R_{\odot}$, they did not trust the result. They quite reasonably suspected that the true error bar was significantly larger than their calculations indicated, because of correlated noise in the data.

This discrepancy was traced by Bakos et al. (2006a) to systematic errors in the OHP photometry. When the B band light curve was recalculated using a greater number of comparison stars, the transit depth decreased by 20% and the inferred planetary radius shrank accordingly.

How does the planetary radius compare to theoretical expectations, given its mass ($M_p = 1.13 \pm 0.03 M_{\text{Jup}}$; Winn et al. 2006) and its proximity to its parent star ($a = 0.035$ AU)? Fortney, Marley, & Barnes (2006) have recently provided a wide range of theoretical predictions for exoplanet radii. Their calculations are for a solar-mass star, but at their suggestion we can rescale the semimajor axis to compensate for the lower luminosity of HD 189733. Assuming $(L_\star/L_\odot) = (M_\star/M_\odot)^{3.5}$, then if HD 189733 were orbiting the Sun at $a = 0.05$ it would receive roughly the same incident flux as it does in its actual orbit. The resulting prediction from Fig. 6 of Fortney et al. (2006) is a planetary radius between ≈ 1.05 – $1.12 R_{\text{Jup}}$, assuming an age of ~ 4.5 Gyr and depending on whether or not the planet has a massive ($25 M_\oplus$) core. The core-free prediction for the radius is larger and in agreement with the observed value. However, it seems premature to claim that a massive core is disfavored, given the uncertainties that enter into the calculations and the uncertainty in the age of the system. It does seem safe to say that the radius of HD 189733 does not present a severe theoretical problem, unlike the cases of the apparently “bloated” planets HD 209458b, HAT-P-1b, and WASP-1b (for recent results on those systems, see Knutson et al. 2006, Bakos et al. 2006b, Collier-Cameron et al. 2006, and Charbonneau et al. 2006b).

The mean density of HD 189733b is $\rho_p = 0.91 \pm 0.06 \text{ g cm}^{-3}$, which is between the densities of Saturn (0.6 g cm^{-3}) and Jupiter (1.2 g cm^{-3}). The surface gravity of HD 189733b is $g = 21 \pm 1 \text{ m s}^{-2}$, which is also intermediate between Saturn (10 m s^{-2}) and Jupiter (25 m s^{-2}). We note that whenever M_p is measured via the spectroscopic orbit of the star, and R_p is measured via transit photometry (as is the case here), then the derived value of g is immune to systematic errors in the parameters of the parent star. This is because the fitting degeneracies are $M_p \propto M_\star^{2/3}$ and $R_p \propto M_\star^{1/3}$, and hence $g \equiv GM_p/R_p^2$ is independent of M_\star . Here this fact is of limited interest, because the error in R_p is dominated by statistical error, but it may be of importance in future transit studies.⁶

4.2. Determination of the Transit Ephemerides

Table 4 gives the 8 transit times measured from our data. We have used these times, along with transit times previously measured by Bakos et al. (2006), to calculate a photometric ephemeris for this system. Although Bakos et. (2006) reported 15 measured times, we used only 4 of those data points in our analysis. We did not include the 10 times that were based on only partial observations of the transit. Full transits are greatly preferable, in order to correct (or at least assess) systematic errors using the pre-ingress and post-egress data. In addition, we did not include

⁶We thank S. Gaudi for helping us to appreciate this point.

the T_c measurement based on the OHP B -band light curve of Bouchy et al. (2005) because of the systematic errors noted previously. What remained were 4 data points representing 4 independent measurements of the same event. In combination with our 8 data points, we fitted a linear function of transit epoch E ,

$$T_c(E) = T_c(0) + EP, \quad (5)$$

finding $T_c(0) = 2453988.80336(23)$ [HJD] and $P = 2.2185733(19)$ days, where the numbers in parentheses indicate the 1σ uncertainty in the final two digits. The fit had $\chi^2/N_{\text{dof}} = 1.08$ and $N_{\text{dof}} = 11$. We chose $E = 0$ to correspond to the most precisely known transit time. Our derived period agrees almost exactly with the value 2.2185730(20) days determined by Bakos et al. (2006a), and it is also in agreement with the *Hipparcos*-based values of 2.2185750(30) days (Bouchy et al. 2005) and $2.218574^{+0.000006}_{-0.000010}$ days (Hébrard & Lecavelier des Estangs 2006).

Figure 4 is the O–C (observed minus calculated) diagram for the transit times, according to this new ephemeris. The filled symbols represent data points used in the fit. There is not yet any pattern in the residuals that would indicate the effect of a perturbing body in the system. The unfilled square shows the OHP B -band measurement, which is indeed an outlier. The unfilled circle is explained in the next section.

4.3. Limits on the Orbital Eccentricity

As mentioned previously, one would expect the orbit of a hot Jupiter such as HD 189733b to be very nearly circular, due to tidal effects. Previous results and our results have all shown that a circular orbit does indeed provide a satisfactory description of the available data. However, it is still interesting to make an empirical determination of the eccentricity, both in the spirit of “what one can measure, one should measure” and also because any additional bodies in the system could excite the orbital eccentricity. We used a two-step procedure to determine the orbital eccentricity.

First, we used our revised ephemeris to interpret the secondary-eclipse timing of Deming et al. (2006). For a nonzero (but small) orbital eccentricity, the time difference between the midpoint of secondary eclipse, T_{sec} , and the time of transit, T_{tra} , may differ from half of the orbital period:

$$T_{\text{sec}} - T_{\text{tra}} \approx \frac{P}{2} \left(1 + \frac{4}{\pi} e \cos \omega \right), \quad (6)$$

where ω is the argument of pericenter. Deming et al. (2006) measured the midpoint of a secondary eclipse at HJD $2453692.62416 \pm 0.00067$, which is consistent with the $e = 0$ prediction of our ephemeris. The unfilled circle in Fig. 4 represents the secondary eclipse measurement. The timing offset of Eq. (6) is 0.46 ± 1.1 minutes, corresponding to $e \cos \omega = 0.00023 \pm 0.00054$.

Second, to determine the other component $e \sin \omega$ of the eccentricity vector, we used the radial velocities presented by Winn et al. (2006). We used only those 60 velocities measured outside of transits (i.e., not affected by the Rossiter-McLaughlin effect). We performed an MCMC analysis to

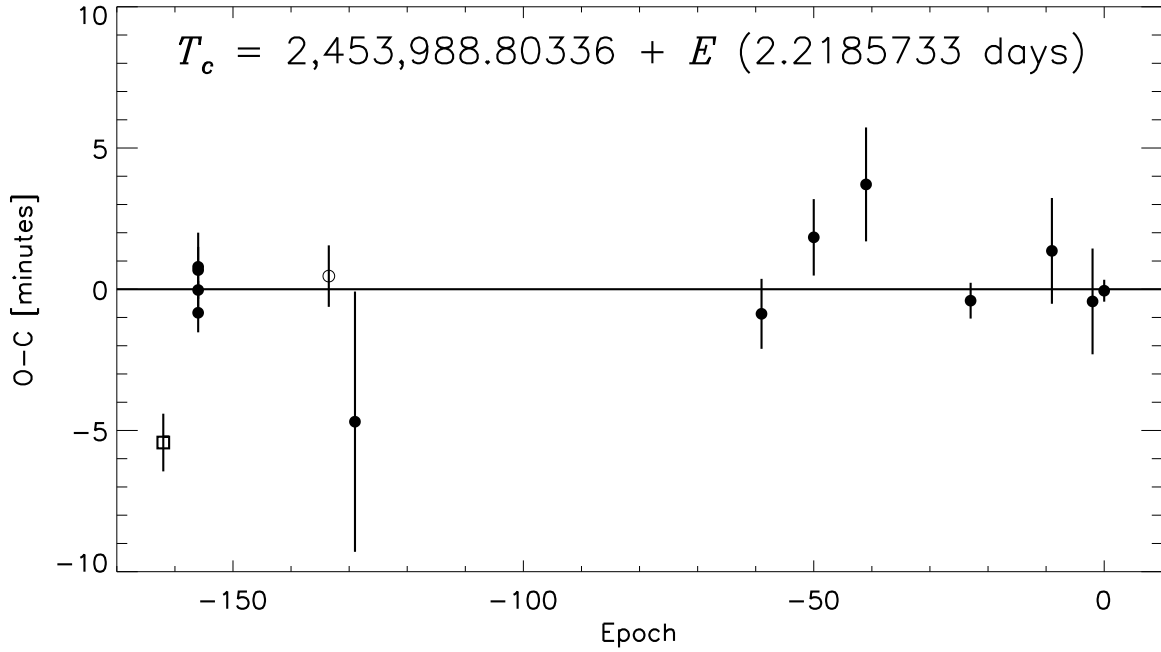


Fig. 4.— Transit and secondary-eclipse timing residuals for HD 189733. The calculated times, using the ephemeris of Eq. (5), have been subtracted from the observed times. The filled symbols represent data points used in the fit. The unfilled square is based on *B*-band data by Bouchy et al. (2005), as re-analyzed by Bakos et al. (2006a). The unfilled circle is the secondary-eclipse time measured by Deming et al. (2006).

solve for the Keplerian orbital parameters, as well as a possible long-term velocity gradient, using the same treatment of the measurement errors that Winn et al. (2006) applied to the entire data set. We allowed both e and ω to be free parameters, but with an a priori constraint on $e \cos \omega$ to enforce compliance with the secondary-eclipse measurement. The result for $e \sin \omega$ was -0.007 ± 0.011 .

Hence, both components of the eccentricity vector are consistent with zero, and $e \cos \omega$ is about 20 times more tightly bounded than $e \sin \omega$. Values of e as large as ≈ 0.02 are allowed, but only for ω very close to $\pm 90^\circ$.

4.4. Three-Dimensional Spin-Orbit Alignment

Thanks to the APT data (§ 2.2), HD 189733 is the first star with a measured rotation period that also has a transiting planet. Together with the transit photometry and the observation of the Rossiter-McLaughlin effect, this allows for the determination of the angle between the stellar rotation axis and the planetary orbit normal, as anticipated by Queloz et al. (2000). This angle is worth measuring because any significant misalignment may be an indication of perturbative effects during planetary migration, among other reasons (as explained in more detail by Ohta et al. 2005, Winn et al. 2005 and Gaudi & Winn 2007).

The true (three-dimensional) angle ψ between the stellar spin axis and the orbital axis is given by the formula

$$\cos \psi = \cos i_\star \cos i + \sin i_\star \sin i \cos \lambda, \quad (7)$$

where i is the orbital inclination, i_\star is the inclination of the stellar rotation axis, and λ is the angle between the sky projections of the two axes. (For a diagram of the coordinate system, see Fig. 3 of Ohta et al. 2005.) The transit photometry determines i with excellent accuracy. Observations of the Rossiter-McLaughlin effect have been used to determine λ , but they cannot be used to determine i_\star independently. Rather, they are sensitive to $v \sin i_\star$, the projected rotation rate of the star. Given $v \sin i_\star$ from the Rossiter-McLaughlin observations⁷, along with i and R_\star from the transit photometry, and the stellar rotation period P_{rot} , one can determine $\sin i_\star$ via the formula

$$\sin i_\star = v \sin i_\star \left(\frac{P_{\text{rot}}}{2\pi R_\star} \right). \quad (8)$$

Hence, all of the angles in Eq. (7) are known. Using the values $\lambda = -1^\circ.4 \pm 1^\circ.1$, and $v \sin i_\star = 2.97 \pm 0.22 \text{ km s}^{-1}$ from Winn et al. (2006), we found $\sin i_\star = 1.04 \pm 0.09$. By rejecting values of $\sin i_\star > 1$ as unphysical, and propagating the errors through Eq. (7), we determined an upper bound on the (mis)alignment angle ψ of 27° with 95% confidence. Essentially the same result can be obtained from the approximation $\cos \psi \approx \sin i_\star$, which is valid because $i \approx 90^\circ$ and $\lambda \approx 0^\circ$ are tightly constrained.

⁷Of course it is also possible to use a more traditional measurement of $v \sin i_\star$, from an analysis of the width of photospheric absorption lines.

This is the first exoplanetary system for which it has been possible to measure ψ . The result is consistent with zero, but it is not as precise as the result for the projected angle λ . How could the measurement of ψ be improved? We have already mentioned some caveats relating to the measurement of the rotation period⁸ (§ 2.2), but the current uncertainty in ψ is dominated by the error in $v \sin i_*$ which is itself dominated by systematic errors arising from the interpretation of the transit spectra (see Winn et al. 2006). Specifically, the systematic error arose from the “calibration” the Rossiter-McLaughlin effect using simulated spectra, which was needed because the transit spectra were observed through an I₂ cell and analyzed with an algorithm that is nominally designed for measuring Doppler shifts rather than spectral distortions. Further improvement might be achieved through a more sophisticated set of simulations or perhaps by re-observing the Rossiter-McLaughlin effect without the I₂ cell (i.e., using a different technique to account for instrumental variations).

5. Summary

We have presented photometry of 8 complete transits of the exoplanet HD 189733b, and modeled the light curves in order to determine the radii of the star and the planet. Our results are consistent with previous results and with theoretical expectations for close-in Jovian planets. Stringent limits on the orbital eccentricity follow from the measured transit times, in conjunction with a previous detection of the secondary eclipse and with the spectroscopic orbit. We have also presented nightly out-of-transit photometry spanning 2 yr that has revealed the stellar rotation period. We have used this information, along with a previous analysis of the spectroscopic transit, to place an upper bound on the true angle between the stellar rotation axis and the orbital axis. With these developments, HD 189733b has become one of the most thoroughly characterized planets outside of the Solar system.

We thank F. Pont and M. Gillon for helpful discussions about correlated noise. We are grateful to G. Marcy, P. Butler, S. Vogt, and E. Turner for their help with the Doppler analysis and for encouragement. A.R. thanks the MIT UROP office for research funding.

REFERENCES

- Adams, F. C., & Laughlin, G. 2006, ApJ, 649, 1004
 Agol, E., Steffen, J., Sari, R., & Clarkson, W. 2005, MNRAS, 359, 567

⁸We note that if the logic in this section is reversed, and one is willing to *assume* perfect spin-orbit alignment, then the calculated rotation period is $P_{\text{rot}} = 12.8 \pm 1.0$ days.

- Bakos, G. Á., et al. 2006, ApJ, in press [astro-ph/0609369]
- Bakos, G. Á., et al. 2006, ApJ, 650, 1160
- Bouchy, F., et al. 2005, A&A, 444, L15
- Butler, R. P., Marcy, G. W., Vogt, S. S., & Apps, K. 1998, PASP, 110, 1389
- Charbonneau, D., Brown, T. M., Latham, D. W., & Mayor, M. 2000, ApJ, 529, L45
- Charbonneau, D., Brown, T. M., Burrows, A., & Laughlin, G. 2006, in Protostars & Planets V, ed. B. Reipurth, D. Jewitt, & K. Keil (Tucson: University of Arizona Press), in press, astro-ph/0603376
- Charbonneau, D., et al. 2006, ApJ, submitted [astro-ph/0610589]
- Claret, A. 2000, A&A, 363, 1081
- Claret 2004, A&A, 428, 1001
- Collier Cameron, A., et al. 2006, MNRAS, in press [astro-ph/0609688]
- Deming, D., Harrington, J., Seager, S., & Richardson, L. J. 2006, ApJ, 644, 560
- Dobbs-Dixon, I., Lin, D. N. C., & Mardling, R. A. 2004, ApJ, 610, 464
- Eaton, J. A., Henry, G. W., & Fekel, F. C. 2003, in The Future of Small Telescopes in the New Millennium, Volume II - The Telescopes We Use, ed. T. D. Oswalt (Dordrecht: Kluwer), 189
- Fortney, J. J., Marley, M. S., & Barnes, J. W. 2006, ApJ, submitted
- Gaudi, B. S., & Winn, J. N. 2007, ApJ, in press [astro-ph/0608071]
- Gelman, A., & Rubin, D. B. 1992, Stat. Sci., 7, 457
- Gillon, M., Pont, F., Moutou, C., Bouchy, F., Courbin, F., Sohy, S., & Magain, P. 2006, A&A, 459, 249
- Hébrard, G., & Lecavelier Des Etangs, A. 2006, A&A, 445, 341
- Henry, G. W. 1999, PASP, 111, 845
- Henry, G. W., Fekel, F. C., & Hall, D. S. 1995, AJ, 110, 2926
- Holman, M. J., & Murray, N. W. 2005, Science, 307, 1288
- Holman, M. J., et al. 2006, ApJ, in press [astro-ph/0607571]
- Holman, M. J., et al. 2006, ApJ, in press [astro-ph/0506569]

- Knutson, H., et al. 2006, preprint [astro-ph/0603542]
- Kobayashi, Y., et al. 1998, Proc. SPIE, 3352, 120
- Mandel, K., & Agol, E. 2002, ApJ, 580, L171
- Masana, E., Jordi, C., & Ribas, I. 2006, A&A, 450, 735
- Minezaki, T., Yoshii, Y., Kobayashi, Y., Enya, K., Sukanuma, M., Tomita, H., Aoki, T., & Peterson, B. A. 2004, ApJ, 600, L35
- Miralda-Escudé, J. 2002, ApJ, 564, 1019
- Ohta, Y., Taruya, A., & Suto, Y. 2005, ApJ, 622, 1118
- Pont, F., Zucker, S., & Queloz, D. 2006, MNRAS, 373, 231
- Rasio, F. A., Tout, C. A., Lubow, S. H., & Livio, M. 1996, ApJ, 470, 1187
- Tegmark, M., et al. 2004, Phys. Rev. D, 69, 103501
- Trilling, D. E. 2000, ApJ, 537, L61
- Yoshii, Y. 2002, in *New Trends in Theoretical and Observational Cosmology*, ed. K. Sato and T. Shiromizu (Tokyo: Universal Academy Press), 235
- Yoshii, Y., Kobayashi, Y., & Minezaki, T. 2003, *Bulletin of the American Astronomical Society*, 35, 752
- Winn, J. N., et al. 2005, ApJ, 631, 1215
- Winn, J. N., et al. 2006, ApJ, 653, L69
- Winn, J. N., et al. 2007, AJ, 133, 11
- Winn, J. N., Holman, M. J., & Roussanova, A. 2006, ApJ, in press [astro-ph/0611404]
- Wright, J. T., Marcy, G. W., Butler, R. P., & Vogt, S. S. 2004, ApJS, 152, 261

Table 1. Characteristics of Transit Data

Date (UT)	Telescope	Filter	Cadence (min)	White Noise σ_w	Red Noise σ_r	Reweighting factor $\sigma_r/(\sigma_w/\sqrt{N_{\text{tr}}})$
2005 Nov 28	T10 APT 0.8m	$(b + y)/2$	1.44	0.0045	0.00250	4.2
2006 May 2	T10 APT 0.8m	$(b + y)/2$	1.44	0.0024	0.00080	2.8
2006 May 22	T10 APT 0.8m	$(b + y)/2$	1.44	0.0024	0.00090	3.0
2006 Jun 11	T10 APT 0.8m	$(b + y)/2$	1.30	0.0019	0.00140	5.3
2006 Jul 21	FLWO 1.2m	z	0.23	0.0023	0.00035	3.3
2006 Aug 21	MAGNUM 2m	V	1.38	0.0029	0.00100	2.9
2006 Sep 5	Wise 1m	I	0.73	0.0029	0.00120	4.6
2006 Sep 10	FLWO 1.2m	z	0.23	0.0022	0.00020	2.0

Table 2. Photometry of HD 189733

HJD	Telescope	Filter	Relative flux	Uncertainty
FLWO 1.2m	z	2453937.71893	1.0037	0.0027
FLWO 1.2m	z	2453937.71909	0.9963	0.0027
FLWO 1.2m	z	2453937.71925	1.0007	0.0027

Note. — The time stamps represent the Heliocentric Julian Date at the time of mid-exposure. We intend for this Table to appear in entirety in the electronic version of the journal. A portion is shown here to illustrate its format. The data are also available from the authors upon request.

Table 3. System Parameters of HD 189733

Parameter	Value	Uncertainty
$(R_\star/R_\odot)(M_\star/0.82 M_\odot)^{-1/3}$	0.753	0.023
$(R_p/R_{\text{Jup}})(M_\star/0.82 M_\odot)^{-1/3}$	1.156	0.044
R_\star/R_\odot	0.753	0.025
R_p/R_{Jup}	1.156	0.046
R_p/R_\star	0.1575	0.0017
$(R_p/a)^2$	0.000313	0.000025
R_\star/a	0.1124	0.0034
i [deg]	85.76	0.29
b	0.658	0.027
$t_{\text{IV}} - t_{\text{I}}$ [hr]	1.827	0.029
$t_{\text{II}} - t_{\text{I}}$ [min]	24.6	1.9

Table 4. Mid-transit times of HD 189733b

Epoch	Mid-transit time	Uncertainty
E	[HJD]	[days]
–129	2453702.60416	0.0032
–59	2453857.90694	0.00086
–50	2453877.87598	0.00094
–41	2453897.84444	0.0014
–23	2453937.77590	0.00044
–9	2453968.83715	0.0013
–2	2453984.36592	0.0013
0	2453988.80331	0.00027